

# A first principles simulation of rigid water

Markus Allesch

*Department of Theoretical Physics, Graz University of Technology, Petersgasse 16, A-8010 Graz, Austria and  
Lawrence Livermore National Laboratory, P.O. Box 808, Livermore, CA 84559*

Eric Schwegler, François Gygi, and Giulia Galli

*Lawrence Livermore National Laboratory, P.O. Box 808, Livermore, CA 84559*

(Dated: November 12, 2018)

We present the results of Car-Parrinello (CP) simulations of water at ambient conditions and under pressure, using a rigid molecule approximation. Throughout our calculations, water molecules were maintained at a fixed intramolecular geometry corresponding to the average structure obtained in fully unconstrained simulations. This allows us to use larger time steps than those adopted in ordinary CP simulations of water, and thus to access longer time scales. In the absence of chemical reactions or dissociation effects, these calculations open the way to *ab initio* simulations of aqueous solutions that require timescales substantially longer than presently feasible (e.g. simulations of hydrophobic solvation). Our results show that structural properties and diffusion coefficients obtained with a rigid model are in better agreement with experiment than those determined with fully flexible simulations. Possible reasons responsible for this improved agreement are discussed.

## I. INTRODUCTION

The importance of water in many areas of science has motivated a large number of experimental and theoretical investigations of the liquid. However, it is only recently that x-ray and neutron diffraction measurements have come to an overall agreement for properties such as the structure of water at ambient conditions<sup>1,2</sup>. In addition, several details of the water structure remain the subject of debate, and many dynamical properties of the liquid are not yet well understood.

Theoretical models have played an important role in the interpretation of experimental measurements and in understanding the physical properties of water<sup>3</sup>. Over the last thirty years, rather accurate empirical force fields have been developed, which can reproduce not only the structure but also many dynamical properties of the liquid<sup>4,5,6</sup>. Although empirical models work well for pure water under ambient conditions, they are usually difficult to generalize to complex solutions or thermodynamic states far from ambient conditions. For example, the majority of empirical water models that are in current use employ potentials that do not change depending on the environment.

In recent years, it has become possible to simulate the properties of a liquid entirely from first principles, without having to resort to fitted potentials. This is due in large part to the development of the Car-Parrinello (CP) method<sup>7</sup> along with the continual increase in high performance computing resources. Although rather accurate and with the potential of being a truly predictive tool, CP simulations are much more computationally intensive than classical simulations.

The case of water is particularly demanding for CP simulations. The ionic vibrational spectrum of the liquid exhibits high frequency modes, i.e. O-H stretch ( $3200$  to  $3600$   $\text{cm}^{-1}$ ) and H-O-H bending modes ( $\sim 1600$   $\text{cm}^{-1}$ ). Therefore, in order to avoid a coupling between the ionic

and electronic degrees of freedom, which could cause severe inaccuracies in a CP simulation, a relatively small fictitious electronic mass ( $\mu \simeq 400$  a.u. for protonated water) needs to be used<sup>8</sup>. In turn, the use of small values of  $\mu$ , together with the high kinetic energy cutoff required to describe the oxygen pseudopotential in a plane wave description, necessitates the use of small integration time steps. The time step may need to be as small as  $0.08$  fs, which is approximately ten times smaller than what is often used in classical MD simulations with empirical inter-atomic potentials. This poses a severe restriction on the time scales that can be accessed in CP simulations of water.

We note that when using Born-Oppenheimer (BO) dynamics (where the total energy of the system is minimized at each ionic step), one can use larger time steps than in CP simulations, since electronic degrees of freedom are not propagated at the same time as ionic coordinates. However, the accuracy required to reduce systematic errors on the ionic forces so as to have conservative dynamics is such that large number of iterations are usually necessary to minimize the Kohn-Sham energy at each ionic step. Therefore, the gain in efficiency obtained with a large time step is more than counter-balanced by the computational time requirement for total energy minimizations.

It is interesting to note that the problem of integrating fast vibrational modes in simulations of liquid water has also been encountered in classical MD simulations, where the most common approach has been to completely eliminate the high-frequency intra-molecular motion by using bond length and angle constraints<sup>9,10</sup>. Based on this approach, a variety of classical water potentials, e.g. the TIP series<sup>6</sup>, are capable of accurately reproducing many of the interesting properties of water. In particular, results obtained with the rigid water TIP5P potential are in very good agreement with a variety of experimental measurements such as the structure, the tempera-

TABLE I: Details of the simulations.

Name	Geometry	$\rho$ (g/cc)	T (K)	dt (fs)	$\mu$ (a.u.)	time (ps)
A	Rigid	0.997	326	0.07	765	16.8
B	Rigid	0.997	315	0.24	1100	24.5
C	Flexible	0.997	291	0.07	340	19.8
D	Rigid	1.570	603	0.07	765	18.6
E	Flexible	1.570	600	0.05	340	3.0

ture of maximum density, diffusion, as well as dielectric properties<sup>6,11,12</sup>.

With the aim of investigating how to increase the integration time step in CP simulations of water and thus access larger time scales, we have carried out calculations using a rigid water approximation. In this paper, we present the results of these simulations and compare them to those obtained with flexible water molecules (i.e. without imposing any constraints on the geometry of the molecules in the liquid), and we discuss the effect of a rigid model on the structural properties of water at ambient and high pressure conditions. Our results show that an *ab initio* rigid water model yields faster diffusion and radial distribution functions which are less structured than those found with a flexible model. Overall, the properties computed with the rigid model are in better agreement with experiment than those determined with a flexible model. Possible reasons for this improved agreement are discussed. In addition, we present a localized orbital analysis of the trajectories obtained with both a rigid and flexible water model, and we demonstrate that the large dipole moment changes in going from the gas to the liquid phase are not significantly altered by the rigid water approximation. The use of a rigid water model in *ab initio* simulations opens the way to much longer simulations of solutions where chemical reactions and dissociation effects do not occur.

## II. METHODS

In order to examine how the structural and dynamical properties of water are altered by a rigid water approximation, we have performed a series of first principle molecular dynamics simulations<sup>13</sup> of water with and without intramolecular bond and angle constraints under ambient and high pressure and temperature conditions. The simulations consist of 54 water molecules in a periodically repeated cubic cell with a lateral dimension of either 11.74 Å or 10.10 Å, which correspond to densities of 1.00 g/cc and 1.57 g/cc, respectively. At each density, we have compared simulations where the intra-molecular geometry of the water molecules are rigid to those where the geometries of the water molecules are fully flexible.

In each simulation, the electronic structure was described within density functional theory (DFT)<sup>14,15</sup> with the PBE generalized gradient approximation<sup>16</sup>. The valence wavefunctions and charge density were expanded

in a plane wave basis, which was truncated in reciprocal space at 85 and 340 Ry, respectively. Norm-conserving pseudopotentials of the Hamman type were used to describe valence-core interactions<sup>17,18</sup>.

The simulations were performed with the CP technique<sup>7</sup>, which is based on the use of a Lagrangian that couples together the system's electronic and ionic degrees of freedom,

$$L_{CP} = \mu \sum_i f_i \int d\mathbf{r} \left| \dot{\Psi}_i(\mathbf{r}) \right|^2 + \frac{1}{2} \sum_I M_I \dot{\mathbf{R}}_I^2 - E_{KS}[\{\Psi_i\}, \mathbf{R}_I] + \sum_{ij} \Lambda_{ij} \left( \int d\mathbf{r} \Psi_i^*(\mathbf{r}) \Psi_j(\mathbf{r}) - \delta_{ij} \right). \quad (1)$$

In Eq. 1,  $\Psi_i(r)$  are the Kohn-Sham orbitals,  $\mu$  is a fictitious mass parameter used to evolve the electronic degrees of freedom in time,  $M_I$  are ion masses,  $E_{KS}$  is the Kohn-Sham energy,  $f_i$  are occupation numbers, and  $\Lambda_{ij}$  are Lagrange multipliers, used to impose the orthonormality constraint  $\int \Psi_i^* \Psi_j = \delta_{ij}$ . The equations of motion derived from Eq. 1 are,

$$\mu \ddot{\Psi}_i(\mathbf{r}, t) = -\frac{\delta E}{\delta \Psi_i^*(\mathbf{r}, t)} + \sum_j \Lambda_{ij} \Psi_j(\mathbf{r}, t) \quad (2)$$

and

$$M_I \ddot{\mathbf{R}}_I = -\frac{\partial E}{\partial \mathbf{R}_I(t)}. \quad (3)$$

Central to the CP method is the introduction of the fictitious mass parameter,  $\mu$ , which enables the electronic and ionic trajectories to be propagated simultaneously at each time step. The particular value of  $\mu$  is chosen so that the dynamics of the electronic degrees of freedom occurs on a time scale that is much faster than, and thus decoupled from, the ion dynamics.

For a given system, an appropriate value of  $\mu$  can be determined by approximating the dynamics of the orbitals generated by Eq. 2 as a superposition of oscillators with frequencies,<sup>19,20</sup>

$$\omega_{ij} = \left[ \frac{2(\epsilon_j - \epsilon_i)}{\mu} \right]^{1/2}, \quad (4)$$

where  $\epsilon_i$  and  $\epsilon_j$  are Kohn-Sham eigenvalues of occupied and unoccupied states, respectively. The lowest frequency obtained from Eq. 4 occurs when  $\epsilon_i$  is the highest occupied state (HOMO) and  $\epsilon_j$  is the lowest unoccupied state (LUMO). As discussed in Ref. 19, although Eq. 4 is a rather crude approximation of the true orbital dynamics, it still provides a useful estimate for selecting an appropriate value of  $\mu$ <sup>8</sup>.

In the case of water, the highest ionic frequency is due to O-H stretching modes, which are at  $\sim 3500$  cm<sup>-1</sup> within density functional theory. In addition, the HOMO-LUMO gap for water within density functional

theory is approximately  $4.6 \text{ eV}^{21}$ . As discussed in Ref. 8, this means that values of  $\mu \sim 340 \text{ au}$  are needed to ensure a clear separation between the ionic and electronic degrees of freedom in CP simulations of flexible, protonated water. However, when the rigid water approximation is used, much larger values of  $\mu$  can be used because the bond distance and angle constraints suppress the high frequency ionic motions. The various values of  $\mu$  that we have used for both the rigid and the flexible water simulations are listed in Table I.

The initial starting configurations of the simulations were generated from previous simulations of flexible water<sup>22</sup> by scaling the intramolecular O-H distances and H-O-H angles, while leaving the spatial orientations of the molecules unchanged. The particular values for the geometry,  $0.9926 \text{ \AA}$  for the O-H distance and  $104.6^\circ$  for the H-O-H angle, were chosen to be the same as the peak values for the intra-molecular O-H distance and H-O-H angular distributions obtained in the previous flexible water simulations<sup>22</sup>. These bond distances and angles are similar to the ones used in the well-known TIP classical water models ( $0.9572 \text{ \AA}$ ,  $104.52^\circ$ )<sup>6</sup>. In order to maintain the distance and angle constraints at every iteration, the SHAKE algorithm was used<sup>23,24</sup>.

In simulations A and B (Table I), the samples were initially heated to a temperature of  $450 \text{ K}$  and cooled to  $300 \text{ K}$  for a period of  $2 \text{ ps}$ . In simulation D, the system was heated to a temperature of  $900 \text{ K}$  and cooled to  $600 \text{ K}$  over  $4 \text{ ps}$ . The thermostats were then removed and the simulations were run under constant energy conditions for the times listed in Table I.

Maximally localized Wannier functions (MLWF)<sup>25,26</sup>, analogous to the orbitals obtained by the Boys localization procedure<sup>27</sup>, were used to determine how the rigid water approximation may influence the electronic structure of the water molecules. By using a recently proposed joint approximate diagonalization scheme, we were able to compute the MLWFs “on-the-fly” for a large number of configurations<sup>28</sup>. Following the procedure proposed by Silvestrelli *et al.*<sup>29</sup>, the centers of the MLWFs have been used to compute an approximate dipole moment of each of the water molecules in the simulation.

### III. RESULTS

The primary effect of the rigid water approximation is best illustrated by comparing the vibrational spectra obtained from a rigid and a flexible water simulation. In Fig. 1, the power spectra collected from simulations A and C are shown. The spectra were computed directly from the velocity autocorrelation function with the maximum entropy method. The two highest frequency modes in the flexible water simulation C are completely absent in simulation A. These modes at  $1600 \text{ cm}^{-1}$  and  $3150 \text{ cm}^{-1}$  correspond to intra-molecular H-O-H bending and O-H stretching, respectively. By suppressing the high frequency modes large values of  $\mu$  can be used, which

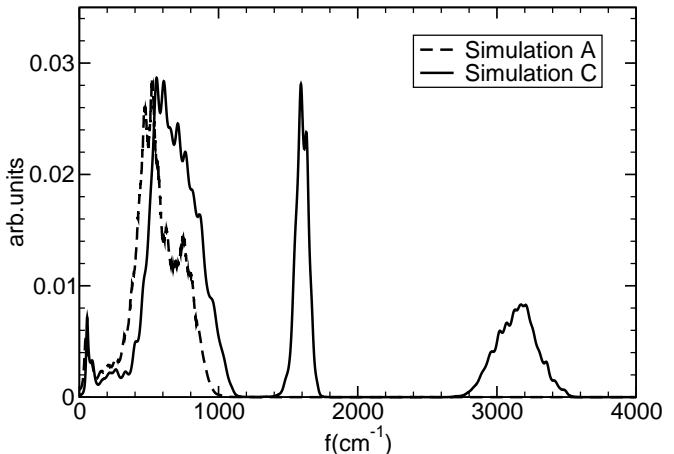


FIG. 1: The computed power spectrum of rigid and flexible liquid water (see text). The dashed line corresponds to the rigid simulation A and the solid line to the flexible simulation C.

in a fully flexible simulation would normally lead to a coupling of the electronic and ionic degrees of freedom, and in turn to a breakdown in the adiabaticity of the CP dynamics<sup>8</sup>.

In addition to the obvious absence of high frequency modes in the rigid water simulation, there are small differences in the lower frequency range of the spectra below  $\sim 1000 \text{ cm}^{-1}$ . For example, the librational modes are slightly shifted to lower frequencies by approximately  $60 \text{ wavenumbers}$  in the rigid water simulation A. Overall, the differences in the low frequency region of the rigid and flexible water simulations are small.

In Fig. 2, the oxygen-oxygen radial distribution functions (RDFs) obtained from simulations A, B and C are shown. Also displayed in Fig. 2, is the latest experimental oxygen-oxygen RDF obtained by an analysis of neutron diffraction data<sup>2</sup>, which is nearly identical to the RDF determined from a recent x-ray diffraction study of water<sup>1</sup>. The small differences between simulations A and B indicate that the choice of  $dt=0.07$  or  $0.24 \text{ fs}$  has little effect on the oxygen-oxygen RDF when the rigid water approximation is used. The differences in the height of the first peak and the first minimum in the RDFs are most likely due to the  $\sim 10 \text{ K}$  higher average temperature of simulation A over simulation B (see Table I). However, as discussed in Ref. 8, for the simulation times used here ( $15\text{-}25 \text{ ps}$ ), differences of this magnitude are within the expected error bars. In Fig. 2 we also show the oxygen-oxygen RDF obtained from simulation C with flexible water molecules. The differences between the rigid and the flexible water simulations are significant. The first peak height is approximately  $0.4$  higher in simulation C than in simulations A and B, and is shifted inward by  $0.03 \text{ \AA}$ . In general, the RDF peak heights and depths are

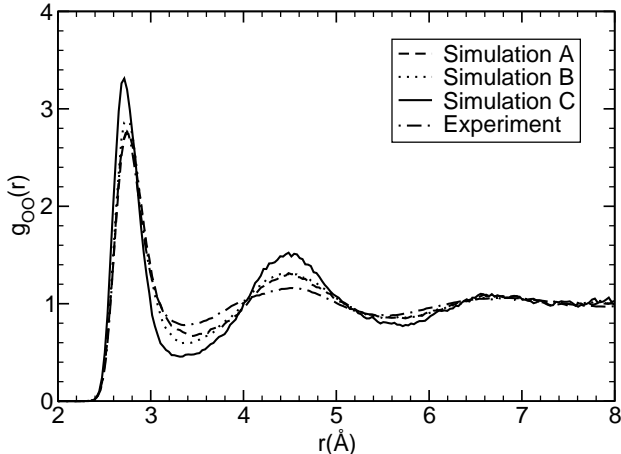


FIG. 2: The oxygen-oxygen radial distribution function of water at ambient conditions. The dashed and dotted lines correspond to the rigid water simulations A and B, respectively, the solid line to the flexible water simulation C, and the dot-dashed line to experiment<sup>2</sup>.

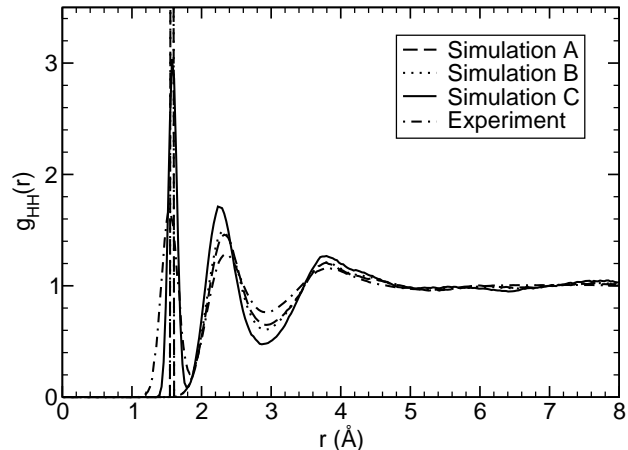


FIG. 4: The hydrogen-hydrogen radial distribution function of water at ambient conditions. The dashed and dotted lines correspond to the rigid water simulations A and B, respectively, the solid line to the flexible water simulation C, and the dot-dashed line to experiment<sup>2</sup>.

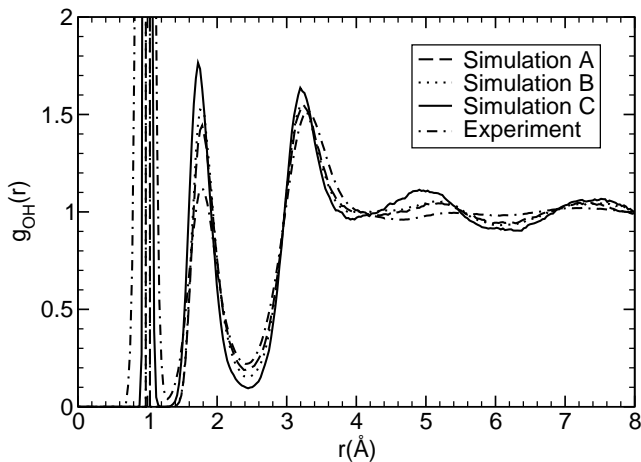


FIG. 3: The oxygen-hydrogen radial distribution function of water at ambient conditions. The dashed and dotted lines correspond to the rigid water simulations A and B, respectively, the solid line to the flexible water simulation C, and the dot-dashed line to experiment<sup>2</sup>.

decreased in the rigid water simulations, showing that the rigid water approximation causes an overall decrease in the structure of the liquid. The same trend in terms of the peak heights and depths has been observed in flexible and rigid water simulations by using the SPC classical interaction potential<sup>30</sup>.

The tendency of the rigid water approximation to decrease the structure of water can also be seen in the

oxygen-hydrogen and the hydrogen-hydrogen RDFs, as shown in Figs. 3 and 4. It is interesting to note that in simulation C the second peak in the oxygen-hydrogen RDF at  $r \sim 2.8$  Å is larger in height than the third peak at  $r \sim 3.2$  Å, whereas in simulations A and B, as well as in the experimental measurement<sup>2</sup>, the second peak is smaller than the corresponding third peak. Since the second oxygen-hydrogen peak coincides with pairs of hydrogen bonded water molecules in the liquid, the relative heights of the second and third peaks have been used as an indicator of the amount of hydrogen bonding in the liquid<sup>30</sup>.

Overall, Figs. 2 to 4 suggest that the main effect of the rigid water approximation is to remove a large fraction of the over-structure that is characteristic of flexible water as described within DFT both by CP<sup>8</sup> and BO molecular dynamics<sup>31</sup>, and in general, the rigid water distribution functions appear to be in better agreement with experiment. There are several possible reasons for this improved agreement. For example, it is possible that the rigid water approximation mimics some of the effects coming from the quantum nature of protons, which are explicitly ignored in simulations that allow for intramolecular flexibility with classical dynamics<sup>30,32,33</sup>. More specifically, in Ref. 32 it was pointed out that at a temperature of 300 K,  $k_B T \sim 200$  cm<sup>-1</sup>, whereas the high frequency intramolecular modes in water range from  $\sim 1000$  to 3500 cm<sup>-1</sup>. In the quantum system the amount of thermal energy available to excite vibrational modes is much smaller than the lowest possible intramolecular vibrational excitations,

$$\hbar\omega \gg k_B T. \quad (5)$$

This indicates that the real quantum system will essentially be restricted to its vibrational ground state at 300 K. Therefore, the quantum system may be better described by a classical rigid water model than by a classical flexible model, despite the fact that in the quantum system the protons become delocalized compared to the classical case.

The effect of the proton quantum motion can be considered with path-integral (PI) methods<sup>34</sup>. To date, all PI simulations with empirical interaction potentials have found an overall softening in the RDFs of water at ambient conditions<sup>11,30,35,36,37</sup>. As pointed out in Ref. 36 these structural changes are quite similar to a 50 K increase in the simulation temperature. However, it is not clear if the lack of quantum effects can fully account for all of the overstructure that appears to be characteristic in the DFT/GGA treatment of water. In addition, a recent PI-DFT simulation<sup>38</sup> has found the surprising result that quantum effects may enhance hydrogen bonding in water.

In order to examine how the dynamical properties of water are affected by the rigid water approximation, we have estimated the diffusion coefficients,  $D$ , for the simulations of rigid and flexible water. To compute the self diffusion coefficient, the mean square displacement (MSD) of the oxygen atoms in the simulations were tracked as a function of the simulation time. The statistical sampling of the simulation data was improved by defining multiple starting configurations separated by 4 fs. The slope of the resulting MSD in the range of 1 to 10 ps was then determined and used to estimate  $D$  according to the Einstein relation<sup>24</sup>,

$$6D_1 = \lim_{t \rightarrow \infty} \frac{d}{dt} \langle |\mathbf{r}_i(t) - \mathbf{r}_i(0)|^2 \rangle. \quad (6)$$

The diffusion coefficient can also be estimated via integration of the oxygen velocity autocorrelation function as

$$D_2 = \frac{1}{3} \int_0^\infty dt \langle \mathbf{v}(t) \cdot \mathbf{v}(0) \rangle, \quad (7)$$

which for the simulation times used here yields nearly identical results as Eq. 6. The measured diffusion coefficients for the different simulations as computed by Eqs. 6 and 7 are reported in Table II. For the rigid water simulations A and B, the diffusion coefficients are approximately 6.2 and 3.2 times larger, respectively, than the flexible water simulation C. Although simulations A and B were both performed at higher temperatures than simulation C, the observed increases in the diffusion coefficients are outside the increase (1.4 to 1.7 fold) expected for a 15 to 26° increase in temperature over ambient, based on experimental data<sup>39</sup>. Given that the rigid water approximation results in a less structured liquid than the flexible one, it is not surprising that it also leads to faster diffusion, which is in closer agreement with the experimental measurement of  $2.4 \times 10^{-5} \text{ cm}^2/\text{s}$ <sup>39,40</sup>.

TABLE II: Summary of computed diffusion coefficients.  $D_1$  corresponds to the diffusion coefficient as estimated by the Einstein relation and  $D_2$  is from integrating the velocity autocorrelation function.

Simulation	$D_1$ ( $10^{-5} \text{ cm}^2/\text{s}$ )	$D_2$ ( $10^{-5} \text{ cm}^2/\text{s}$ )
A	2.5	2.4
B	1.3	1.2
C	0.3	0.4
D	2.5	2.5

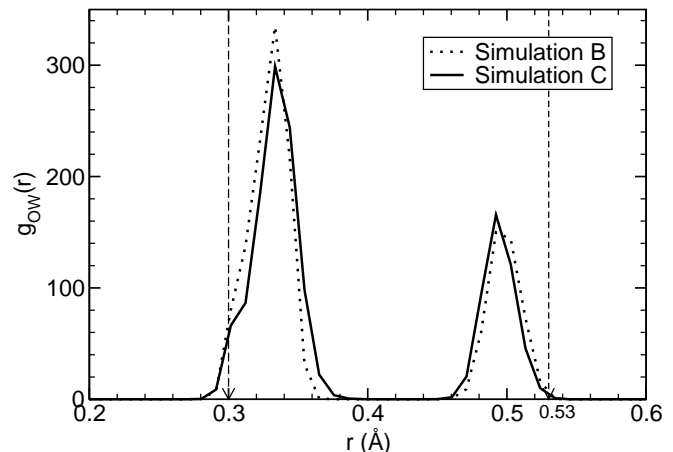


FIG. 5: The oxygen-MLWF center radial distribution function for rigid and flexible water. The dotted line corresponds to the rigid simulation B and the solid line to the flexible simulation C. The dashed vertical lines represent the location of MLWFs for an isolated water molecule.

In addition to possible changes in structure and dynamics, we have examined how the rigid molecule approximation changes the electronic properties of water. In order to do this we have performed a localized orbital analysis by computing the MLWFs for a series of well-separated snapshots from the rigid water simulation B and the flexible water simulation C. Within the pseudopotential approximation, there are four doubly occupied MLWFs around each of the water molecules in the simulations. Two of the MLWFs are localized on the oxygen-hydrogen covalent bonds, and the other two are localized on the lone-pair locations of the oxygen atoms. Given the large amount of data that the MLWFs represent, in the following, we only consider the centers of the MLWFs rather than the orbitals themselves. In Fig. 5, the oxygen-MLWF center RDFs for simulations B and C are shown. The RDFs consist of two distinct distributions centered at  $r \sim 0.33 \text{ \AA}$  and  $r \sim 0.49 \text{ \AA}$ , which correspond to lone-pair and covalent bond locations, respectively. For comparison, the dashed vertical lines in Fig. 5 represent the locations of the MLWF centers around the

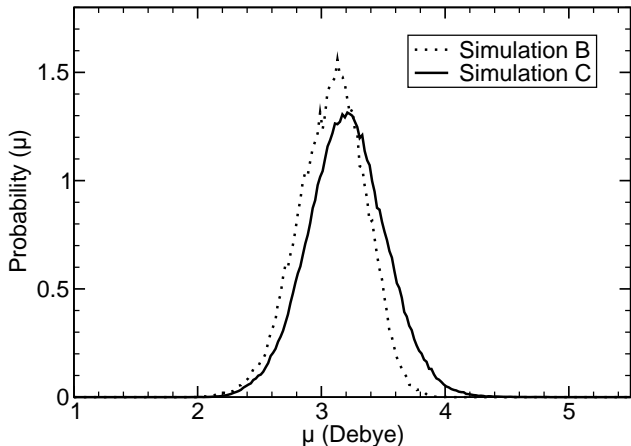


FIG. 6: The probability distribution of molecular dipole moments of water computed from MLWF centers. The dotted line corresponds to the rigid simulation B and the solid line to the flexible simulation C.

oxygen atom of an isolated gas phase water molecule. Surprisingly, the rigid water approximation does not significantly alter the large changes in the MLWF centers that are expected when going from an isolated water molecule to the liquid state. As can be seen in Fig. 5, the lone pair distributions are shifted away from the oxygen atoms by  $\sim 0.03$  Å, and the covalent bond distributions are shifted toward the oxygen atoms by  $\sim 0.04$  Å.

As proposed by Silvestrelli *et al.*<sup>29</sup>, an approximate dipole moment for each water molecule in the liquid can be defined by assigning the total charge of each MLWF to a point charge located at its corresponding center. Because the MLWF on neighboring water molecules in the liquid do not significantly overlap, this provides a less ambiguous definition of the molecular dipole moments than arbitrarily assigning electron density to individual water molecules. As pointed out in Ref. 41, dipole moments computed in this manner from static configurations may not be representative of the experimentally measured dipole moments in the fluid. However, the MLWF dipole moments are useful for examining qualitative differences in the polarization of water as a function of different approximations or of solutes present in the liquid.

In Fig. 6, the probability distributions of molecular dipole moments for rigid and flexible water systems calculated from the MLWF centers are shown. Fig. 6 indicates that the rigid water approximation has a rather small effect on distribution of dipole moments in the liquid. In particular, the average moment in simulation B is shifted to 3.08 Debye as compared to 3.20 Debye in simulation C. Apparently, an explicit description of high frequency O-H stretch and H-O-H bending modes is not necessary to reproduce the broad range of moments that are charac-

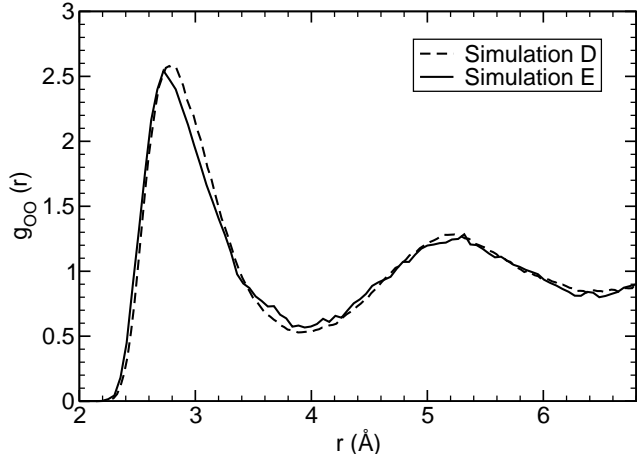


FIG. 7: The oxygen-oxygen radial distribution function of water at  $\rho=1.57$  g/cc. The dashed line is from the rigid water simulation D, and the solid line is from the flexible water simulation E.

teristic of the liquid. It is also interesting to note that the latest experimental estimate based on an analysis of the x-ray structure factor of water indicates that the dipole moment of water in the liquid is 2.9 Debye<sup>42</sup>, which is in closer agreement with the rigid water model than the flexible simulation.

The decrease in the average dipole moment obtained from the rigid water approximation offers another explanation for the observed softening of the liquid structure. In addition to mimicking quantum effects, it is possible that the rigid water approximation to some extent corrects for the general tendency of simple GGA-based functionals to overestimate the polarizability of molecules<sup>43,44,45,46</sup>. For example, the static isotropic polarizability of an isolated water molecule is 10.74 au with the PBE functional as compared to the experimental value of 9.64 au<sup>46</sup>. It is interesting to note that hybrid DFT functionals, which include some amount of Hartree-Fock exchange, appear to significantly improve on the polarizability of water. In particular, the average polarizability of the water molecule is 9.78 au with hybrid PBE0 functional<sup>46</sup>.

In addition to water under ambient conditions, we have also examined how the rigid water approximation affects the properties of water under extreme temperatures and pressures. In particular, we have performed a simulation of rigid water (simulation D) and of flexible water (simulation E) at a density of 1.57 g/cc and an average temperature of  $\sim 600$  K. These high density and temperature conditions correspond to a regime where molecular dissociation is still considered a rare event<sup>22,47</sup>. However, the pressure ( $\sim 10$  GPa) is high enough to cause a large increase in the nearest neighbor coordination of each water from 4.5 at ambient conditions to nearly 13 at

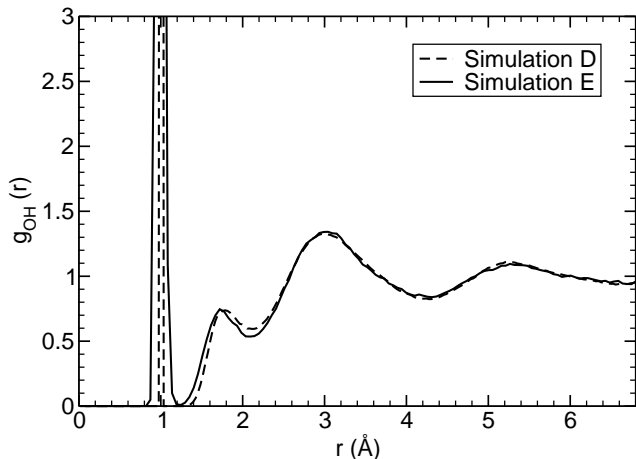


FIG. 8: The oxygen-hydrogen radial distribution function of water at  $\rho=1.57$  g/cc. The dashed line is from the rigid water simulation D, and the solid line is from the flexible water simulation E.

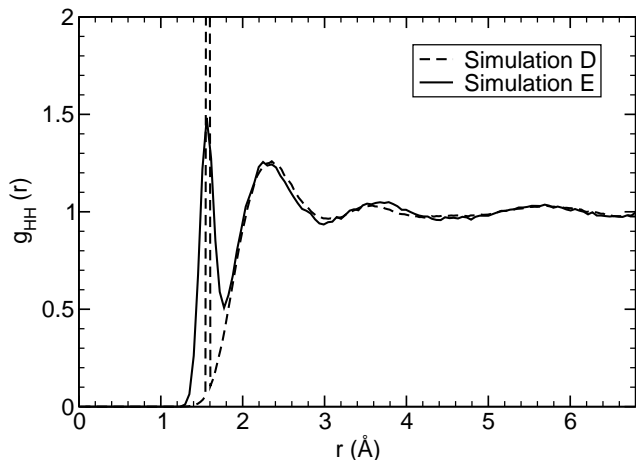


FIG. 9: The hydrogen-hydrogen radial distribution function of water at  $\rho=1.57$  g/cc. The dashed line is from the rigid water simulation D, and the solid line is from the flexible water simulation E.

high pressure<sup>47</sup>. The oxygen-oxygen, oxygen-hydrogen and hydrogen-hydrogen RDFs for simulations D and E are compared in Figs. 7 to 9. Except for the expected intramolecular differences due to the constraints, the RDFs obtained from simulations D and E are remarkably simi-

lar. In particular, both the large increase in the number of nearest neighbors as well as the stiffness of the first peak in  $g_{OO}(r)$  as a function of compression are reproduced by the rigid water model<sup>47</sup>. As higher densities and temperatures are considered, intramolecular dissociation will become a common event in flexible water simulations<sup>22</sup> and the rigid water approximation is expected to be inappropriate for the description of the liquid.

#### IV. CONCLUSION

In summary, we have used a series of Car-Parrinello molecular dynamics simulations to examine how the rigid water approximation affects the computed properties of water in the liquid state at ambient conditions. In agreement with previous observations based on empirical interaction potentials<sup>30</sup>, the rigid water approximation is found to cause an overall decrease in structure and an increase in diffusion of the liquid. These changes result in properties that are in better agreement with experimental measurements than the corresponding first principles simulations with flexible water molecules. At higher temperatures and densities in a regime where intramolecular dissociation is still a rare event, the differences between simulations where water molecules are either rigid or flexible become negligible.

In addition to an improved structural and dynamical description of water, the rigid water model enables the use of time steps as large as 0.24 fs within the Car-Parrinello scheme (i.e.  $\sim 3$  times larger than in a flexible water simulation). A similar conclusion was reached in Ref. 48 for first-principle simulations of a cytosine molecule in the gas phase. This represents an important advantage for first-principle simulations of aqueous solutions where chemical reactions do not occur, and opens up the possibility of investigating phenomena that take place on a long timescale. For example, understanding how water orients around a hydrophobic solute may require simulations of the order of 100 to 200 ps. The rigid water approximation presented here may prove to be an accurate and efficient approach for describing the interaction between a hydrophobic solute and water within a first-principles context.

The authors would like to thank J. C. Grossman for many useful discussions. This work was performed under the auspices of the U.S. Dept. of Energy at the University of California/Lawrence Livermore National Laboratory under contract no. W-7405-Eng-48.

<sup>1</sup> J. M. Sorenson, G. Hura, R. M. Glaeser, and T. Head-Gordon, *J. Chem. Phys.* **113**, 9149 (2000).

<sup>2</sup> A. K. Soper, *Chem. Phys.* **258**, 121 (2000).

- <sup>3</sup> B. Guillot, *J. Mol. Liq.* **101**, 219 (2002).
- <sup>4</sup> F. H. Stillinger and A. Rahman, *J. Chem. Phys.* **60**, 1545 (1974).
- <sup>5</sup> H. J. C. Berendsen, J. P. M. Postma, and W. F. van Gunsteren, in *Intermolecular Forces*, edited by B. Pullman (Reidel, Dordrecht, 1981), p. 331.
- <sup>6</sup> M. W. Mahoney and W. L. Jorgensen, *J. Chem. Phys.* **112**, 8910 (2000).
- <sup>7</sup> R. Car and M. Parrinello, *Phys. Rev. Lett.* **55**, 2471 (1985).
- <sup>8</sup> J. C. Grossman *et al.*, *J. Chem. Phys.* accepted for publication (2003).
- <sup>9</sup> W. F. van Gunsteren and M. Karplus, *Macromolecules* **15**, 1528 (1982).
- <sup>10</sup> T. Schlick, E. Barth, and M. Mandziuk, *Annu. Rev. Biophys. Biomol. Struct.* **26**, 181 (1997).
- <sup>11</sup> M. W. Mahoney and W. L. Jorgensen, *J. Chem. Phys.* **115**, 10758 (2001).
- <sup>12</sup> M. W. Mahoney and W. L. Jorgensen, *J. Chem. Phys.* **114**, 363 (2001).
- <sup>13</sup> F. Gygi, *GP 1.24.0: A general ab initio molecular dynamics program*, Lawrence Livermore National Laboratory, 2003.
- <sup>14</sup> P. Hohenberg and W. Kohn, *Phys. Rev. B* **136**, 864 (1964).
- <sup>15</sup> W. Kohn and L. J. Sham, *Phys. Rev. A* **140**, 1133 (1965).
- <sup>16</sup> J. P. Perdew, K. Burke, and M. Ernzerhof, *Phys. Rev. Lett.* **80**, 891 (1998).
- <sup>17</sup> D. R. Hamann, *Phys. Rev. B* **40**, 2980 (1989).
- <sup>18</sup> L. Kleinman and D. M. Bylander, *Phys. Rev. Lett.* **48**, 1425 (1982).
- <sup>19</sup> G. Pastore, E. Smargiassi, and F. Buda, *Phys. Rev. A* **44**, 6334 (1991).
- <sup>20</sup> G. Galli and M. Parrinello, in *Computer Simulation in Materials Science*, edited by M. Meyer and V. Pontikis (Kluwer Academic Publishers, Netherlands, 1991), pp. 283–304.
- <sup>21</sup> K. Laasonen, M. Sprik, and M. Parrinello, *J. Chem. Phys.* **99**, 9080 (1993).
- <sup>22</sup> E. Schwegler, G. Galli, F. Gygi, and R. Q. Hood, *Phys. Rev. Lett.* **87**, 265501 (2001).
- <sup>23</sup> J. P. Ryckaert, G. Ciccotti, and H. J. C. Berendsen, *J. Comput. Phys.* **23**, 327 (1977).
- <sup>24</sup> M. P. Allen and D. J. Tildesley, *Computer Simulation of Liquids* (Clarendon Press, Oxford, 1987).
- <sup>25</sup> N. Marzari and D. Vanderbilt, *Phys. Rev. B* **56**, 12847 (1997).
- <sup>26</sup> P. L. Silvestrelli, N. Marzari, D. Vanderbilt, and M. Parrinello, *Solid State Commun.* **107**, 7 (1998).
- <sup>27</sup> S. F. Boys, *Rev. Mod. Phys.* **32**, 296 (1960).
- <sup>28</sup> F. Gygi, J. L. Fattebert, and E. Schwegler, *Comp. Phys. Comm.* **155**, 1 (2003).
- <sup>29</sup> P. L. Silvestrelli and M. Parrinello, *Phys. Rev. Lett.* **82**, 3308 (1999).
- <sup>30</sup> J. Lobaugh and G. A. Voth, *J. Chem. Phys.* **106**, 2400 (1997).
- <sup>31</sup> D. Asthagiri, L. R. Pratt, and J. D. Kress, *Phys. Rev. E* **68**, 041505 (2003).
- <sup>32</sup> I. G. Tironi, R. M. Brunne, and W. F. van Gunsteren, *Chem. Phys. Lett.* **250**, 19 (1996).
- <sup>33</sup> B. Hess, H. Saint-Martin, and H. J. C. Berendsen, *J. Chem. Phys.* **116**, 9602 (2002).
- <sup>34</sup> R. P. Feynman and A. R. Hibbs, *Quantum Mechanics and Path Integrals* (McGraw Hill, New York, 1965).
- <sup>35</sup> R. A. Kuharski and P. J. Rossky, *J. Chem. Phys.* **82**, 5164 (1985).
- <sup>36</sup> G. S. D. Buono, P. J. Rossky, and J. Schnitker, *J. Chem. Phys.* **95**, 3728 (1991).
- <sup>37</sup> H. A. Stern and B. J. Berne, *J. Chem. Phys.* **115**, 7622 (2001).
- <sup>38</sup> B. Chen, I. Ivanov, M. L. Klein, and M. Parrinello, *Phys. Rev. Lett.* **91**, 215503 (2003).
- <sup>39</sup> K. Krynicki, C. D. Green, and D. W. Sawyer, *Faraday Disc. Chem. Soc.* **66**, 199 (1978).
- <sup>40</sup> R. Mills, *J. Phys. Chem.* **77**, 685 (1973).
- <sup>41</sup> A. Pasquarello and R. Resta, *Phys. Rev. B* accepted for publication (2003).
- <sup>42</sup> Y. S. Badyal *et al.*, *J. Chem. Phys.* **112**, 9206 (2000).
- <sup>43</sup> S. A. C. McDowell, R. D. Amos, and N. C. Handy, *Chem. Phys. Lett.* **235**, 1 (1995).
- <sup>44</sup> P. Calaminici, K. Jug, and A. M. Köster, *J. Chem. Phys.* **109**, 7756 (1998).
- <sup>45</sup> A. J. Cohen and Y. Tantirungrotechai, *Chem. Phys. Lett.* **299**, 465 (1999).
- <sup>46</sup> C. V. Caillie and R. D. Amos, *Chem. Phys. Lett.* **328**, 446 (2000).
- <sup>47</sup> E. Schwegler, G. Galli, and F. Gygi, *Phys. Rev. Lett.* **84**, 2429 (2000).
- <sup>48</sup> E. Tsuchida and K. Terakura, *J. Phys. Soc. Japan* **70**, 924 (2001).